Nanoporous polyethylene microfibres for large-scale radiative cooling fabric

Yucan Peng [1,5], Jun Chen [1,5], Alex Y. Song [2,5], Peter B. Catrysse[2,5], Po-Chun Hsu[3], Lili Cai[1], Bofei Liu[1], Yangying Zhu[1], Guangmin Zhou[1], David S. Wu[1], Hye Ryoung Lee[1], Shanhui Fan[2] and Yi Cui[1,4]*

Global warming and energy crises severely limit the ability of human civilization to develop along a sustainable path. Increasing renewable energy sources and decreasing energy consumption are fundamental steps to achieve sustainability. Technological innovations that allow energy-saving behaviour can support sustainable development pathways. Energy-saving fabrics with a superior cooling effect and satisfactory wearability properties provide a novel way of saving the energy used by indoor cooling systems. Here, we report the large-scale extrusion of uniform and continuous nanoporous polyethylene (nanoPE) microfibres with cotton-like softness for industrial fabric production. The nanopores embedded in the fibre effectively scatter visible light to make it opaque without compromising the mid-infrared transparency. Moreover, using industrial machines, the nanoPE microfibres are utilized to mass produce fabrics. Compared with commercial cotton fabric of the same thickness, the nanoPE fabric exhibits a great cooling power, lowering the human skin temperature by 2.3 °C, which corresponds to a greater than 20% saving on indoor cooling energy. Besides the superior cooling effect, the nanoPE fabric also displays impressive wearability and durability. As a result, nanoPE microfibres represent basic building blocks to revolutionize fabrics for human body cooling and pave an innovative way to sustainable energy.

Nowadays, problems associated with energy crises and climate change are becoming increasingly serious stumbling blocks for human sustainable development[1–4]. Fifteen per cent of electricity consumption and ten per cent of greenhouse gas emissions are ascribed to cooling systems globally[5]. Therefore, developing new technologies to reduce the energy demand for spacing heating and cooling is significant for energy saving. Notably, an increase in the cooling set-point of 2 °C can save over 20% of energy for indoor temperature regulation[6].

Without wasting excess energy on the entire building[7–9], personal thermal management emphasizing heating and cooling of only the human body and its local environment is more energy-efficient and cost-effective[10–12]. In a typical indoor environment, the human body with a normal skin temperature of about 33.5 °C emits mid-infrared thermal radiation in the wavelength range of 7 to 14 μm, accounting for over 50% of the total body heat loss[13] (see Supplementary Note 1 and Supplementary Figs. 1 and 2 for more details). Recently, we demonstrated effective radiative human body cooling using a nanoporous polyethylene (nanoPE) non-woven thin film due to its superior mid-infrared transparency and high opacity to visible light[11]. However, polymer thin film is by nature unsuitable for normal clothing, because it lacks essential wearable properties, such as air permeability and touch comfort. For instance, the polyethylene thin film is very electronegative while human skin is electropositive; thus, a strong contact electrification would be induced during wearing[14], which would result in great discomfort. These concerns can be well resolved by developing knitted/woven fabric using nanoPE microfibres with cotton-like softness as the building blocks.

The knitted/woven structure in fabric holds several advantages for wearing. First, it contains hierarchical pores, ranging from hundreds of micrometres to submicrometres. As air permeability is quadratically proportional to the pore diameter[15], the large pores resulting from the knitted/woven configuration would dominate the air permeability, rendering it as air-permeable as a cotton fabric. Meanwhile, the large pores can also benefit convective cooling, because heat exchange via air convection can easily happen between the skin and the ambient environment. Second, the knitted/woven structure enables the fabric to be more stretchable. Fibres with interlaced structure can undergo much more strain than a straight one of the same material[16–18]. Third, knitted/woven fabrics tend to show better mechanical strength. When force is applied to a fabric, the ordered interlaced structure can effectively transfer the applied load around with uniform distribution on the fabric (Supplementary Fig. 3). Besides, the knitted/woven fabric can greatly decrease the electrification and irreversible wrinkling compared to the nanoPE thin film (Supplementary Videos 1 and 2), which is also very critical toward comfortable wearing.

Accordingly, to realize practical radiative human body cooling and renovate the human cloth toward a sustainable civilization, developing a new process for massive production of nanoPE microfibres as the building blocks for large-scale fabric manufacture is a must. Although polyethylene is currently obtained from fossil fuels, further innovation of plastic production will amplify the sustainability potential of such cooling fabric. Moreover, nanoPE fabric can be easily recycled by melting and re-extrusion for new clothing manufacture.

NanoPE microfibre
To bring the real impact into human society, large-scale production of high-quality nanoPE microfibres is the cornerstone and first step. Normal polyethylene (PE) fibres, such as gel-spun ultrahigh-molecular-weight PE fibre and melt-spun high-density

polyethylene (HDPE) fibre, are widely used as ropes, cables and ballistic-resistant composites due to their high mechanical strength and chemical resistance[19–21]. However, normal PE fibres cannot be used for next-to-skin fabric due to their mechanical stiffness and visible transparency. To obtain a cooling fabric with satisfactory wearability, here we propose to introduce nanoscale porosities into PE microfibres via large-scale fabrication techniques. This crucial innovation generates two functions simultaneously: an optical function, where the nanoscale pores (100 nm to 1,000 nm) scatter visible light (400–700 nm in wavelength) strongly while permitting mid-infrared light (7 to 14 μm) to transmit, creating the necessary optical effect of visible opacity and mid-infrared transparency; and a mechanical function, where the nanoscale pores reduce the mass occupation of PE inside the microfibres and create a lot of localized empty space to accommodate the bending motion of the microfibres. The mechanical hardness of solid microfibres can be reduced significantly when modified into nanoporous microfibres, making PE materials soft to wear.

However, no nanoPE fibres for fabric have been reported to date. PE is a very chemically inert material and is not soluble in most solvents. To create nanoPE, we invent a new process to manufacture the nanoPE fibres. Paraffin oil is selected as the solvent for PE because it has chemical properties similar to PE, which consists of nonpolar, saturated, high-molecular-weight hydrocarbons[22]. The properties in common make them compatible with each other at a suitable temperature (180 °C) and they form a highly viscous homogeneous solution, which can be continuously extruded by an industrial extruder machine to form fibres with microscale diameters. Once extruded, the oily PE fibre cools down fast, and then solid-phase PE is separated out from the liquid-phase paraffin oil. The phase separation process creates nanoscale domains of oil intermixed together with PE. Subsequently, methylene chloride, which can selectively resolve paraffin oil, is used to extract the oil phase from the oily PE fibres. The removal of the oil phase leaves a nanoporous space embedded into the PE solid matrix, generating nanoPE microfibres. The whole procedure is illustrated in Fig. 1a. Supplementary Fig. 4 shows a photograph of the extruder producing nanoPE microfibres, which can be continuously produced with satisfactory uniformity and mechanical strength at a speed of about 50 metres per minute (Supplementary Video 3). As detailed in the Methods, the production of the nanoPE microfibres is straightforward and compatible with large-scale manufacturing.

Spools of nanoPE microfibres are mass produced by large-scale extrusion not only in the laboratory (Supplementary Fig. 5), but also in industry (Fig. 1b). The inset of Fig. 1b shows an array of nanoPE microfibres in milky white colour with cotton-like softness (Supplementary Video 4). Figure 1c compares the appearance of nanoPE fibres and normal PE fibres in the same image using an optical microscope. The nanopores in nanoPE fibres can scatter visible light strongly and render the nanoPE fibre milky white in colour, whereas the normal PE fibre looks visibly transparent. Scanning electron microscope (SEM) images of the surface (Fig. 1d) and a cross-section view (Fig. 1e) of a nanoPE microfibre show that the nanoscale cavities are contiguous with each other from the inner surface to the outer fibre surface. The inset of Fig. 1e is a lower-magnification SEM image showing the well-preserved cross-section of the microfibre. The sizes of these nanoscale cavities (100 nm–1,000 nm) are too small to scatter mid-infrared light (7–14 μm), but are perfect for scattering visible light (400–700 nm) to realize the opacity. Moreover, the nanoscale pores embedded in the microfibre can easily alter their shapes to adapt to the bending of the microfibre, as illustrated in Fig. 1f. This is the reason why the nanoPE microfibre has cotton-like softness, whereas the normal PE microfibre is much more rigid (Supplementary Fig. 6).

To control the pore size and fibre porosity, the ratio of PE and paraffin oil plays a key role. Normal PE microfibre is transparent with a smooth surface. As for nanoPE microfibres, the pore size and porosity increase as the oil ratio increases. When the paraffin oil ratio is low, the droplets of oil can distribute in the solid PE matrix as tiny separate domains. As the paraffin oil ratio increases, tiny droplets of paraffin oil tend to distribute as contiguous nanoscale oil domains, and eventually form an interconnected matrix within the solid PE system, as demonstrated in Supplementary Figs. 7 and 8.

The ratio of PE and paraffin oil is also critical for the mechanical strength and softness of the nanoPE microfibres. As shown in Supplementary Fig. 9, the tensile strength of the nanoPE microfibres depends on the ratio of paraffin oil to PE. Generally, with a higher ratio of paraffin oil to PE, the nanopore volume fraction in the nanoPE microfibres increases. This would greatly improve the fibre softness, but reduce its mechanical strength. Conversely, with a lower ratio of paraffin oil to PE, fewer nanoscale cavities would be formed in the obtained microfibre, which gives it a higher mechanical strength. However, the low porosity would lead to visible translucence and large stiffness, which can greatly reduce the feasibility and comfort for wearing. Namely, a trade-off exists between the fibre softness and mechanical strength. Experimentally, a ratio of 1:3.5 (PE weight/oil volume) is tested as the optimized recipe to deliver a satisfactory mechanical strength together with cotton-like softness.

Industrial-scale textile fabrication

Tens of pounds of nanoPE microfibres can be rapidly and continuously produced via the fibre extrusion process. Consequently, nanoPE fabrics are efficiently realized via industrial knitting/weaving equipment. As illustrated in Fig. 2a, the nanoPE fabric not only maintains high mid-infrared transmittance and visible opacity, but also greatly improves the wearability. The achievement mainly originates from two aspects: fabrication of nanoPE microfibres and adoption of a knitted/woven structure. Figure 2b exhibits a piece of woven nanoPE fabric with a dimension of 1.8 m by 0.5 m. An enlarged view of the fabric, to show its woven structure, is demonstrated in Fig. 2c. Besides woven fabric, the nanoPE microfibres are also demonstrated to construct a fabric via knitting (Fig. 2d). In such knitted nanoPE fabric, the nanoPE fibre loops are interlocked with each other, forming an ordered knitted structure (Fig. 2e). In contrast, the appearance of the nanoPE thin film is similar to a piece of plastic film with randomly distributed disordered nanoscale branches, as the sketch, photograph and SEM image show in Supplementary Fig. 10.

Optical and thermal properties

The visible opacity of the nanoPE fabric, using the knitted one as an example, is measured with an ultraviolet–visible spectrometer. Opacity is defined as (1 − specular transmittance). As demonstrated in Fig. 3a, the nanoPE fabric shows visible opacity of nearly 90%. Although this number is a little lower than that of the nanoPE thin film, cotton fabric and Tyvek, it is reasonably good for wearing. In addition, as shown in the inset, ascribed to the light scattering by the nanopores, the nanoPE fabric is much more visibly opaque than the fabric made of normal PE fibres. However, the latter still displays some opacity, because the interlaced structure contributes to additional opacity compared to a flat normal PE film. According to the simulation via Mie theory (Supplementary Fig. 11), the opacity of knitted fabric can reach up to 54% even for those made of transparent normal PE fibres, indicating the extra contribution of the knitted structure to visible opacity.

The total infrared light transmittance is investigated with a Fourier transform infrared (FTIR) spectrometer equipped with a diffuse gold integrating sphere, to characterize mid-infrared transparency of the nanoPE fabric. The experimentally measured mid-infrared transmittance is shown in Fig. 3b. The nanoPE thin film exhibits the highest infrared transmittance owing to it having the
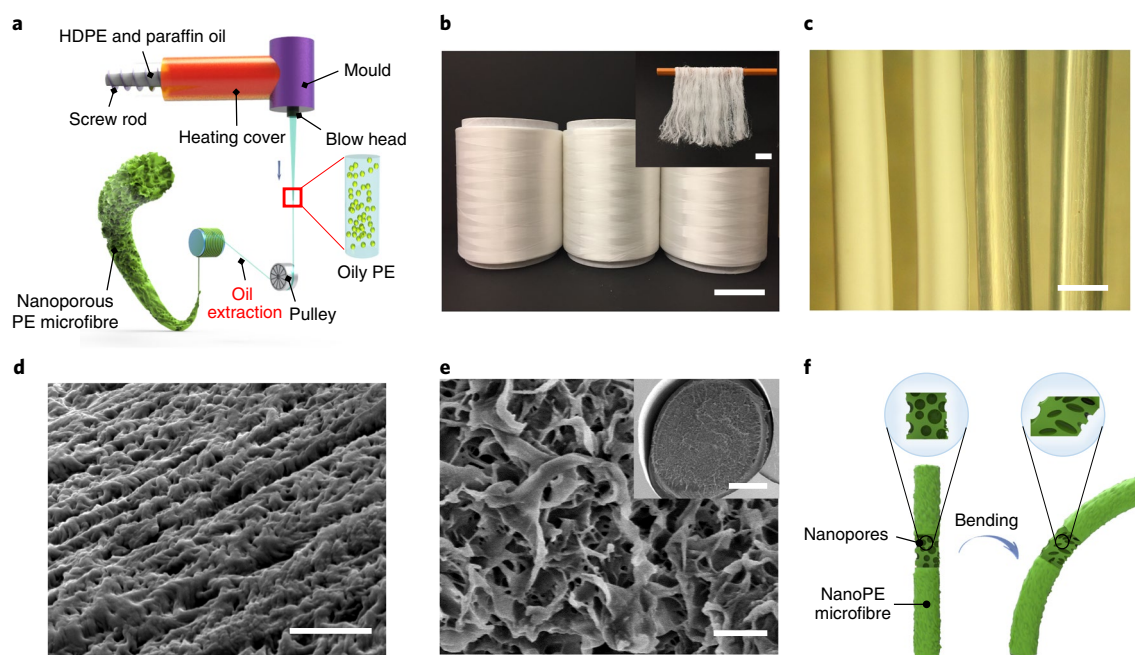
Fig. 1 | NanoPE microfibre. a, A schematic diagram of the manufacturing process for the nanoPE microfibre. **b**, A photograph of three spools of nanoPE microfibres produced by industrial extrusion. Scale bar, 9 cm. The inset shows that the fibres are milky white with cotton-like softness. Scale bar, 1.5 cm. **c**, An optical micrograph of a nanoPE microfibre (left) and a normal PE fibre (right). The white colour of the nanoPE microfibre is mainly attributed to the strong visible light scattering by the embedded nanoscale cavities, while normal PE looks transparent under visible light. Scale bar, 200 μm. **d**, SEM image of the surface of a nanoPE microfibre. Scale bar, 2 μm. **e**, SEM image of the cross-section view of a nanoPE microfibre. Scale bar, 2 μm. The inset shows a lower-magnification SEM image of the well-preserved cross-section of the microfibre. Scale bar, 50 μm. **f**, An illustration showing the nanoscale porosities adapting to a bent deformation, thereby improving the softness for wearing.
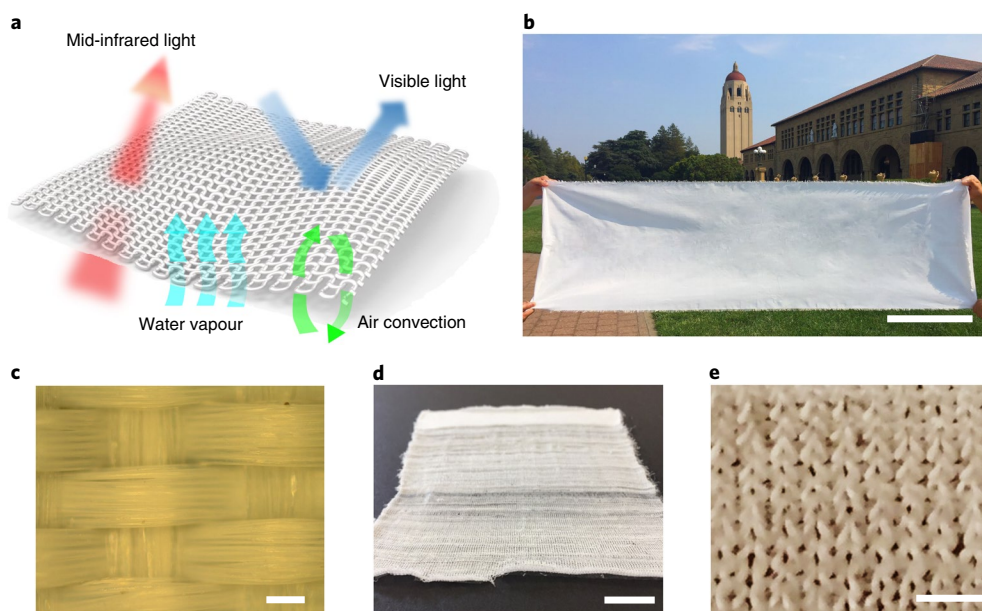

Fig. 2 | NanoPE fabrics. a, A schematic diagram of the nanoPE fabric. The nanoPE fabric exhibits high mid-infrared transparency, visible opacity and good wearability. **b**, A photograph of a large woven nanoPE fabric. Scale bar, 0.35 m. **c**, An enlarged view of the woven nanoPE fabric showing the woven structure. Scale bar, 200 μm. **d**, A photograph of a knitted nanoPE fabric. Scale bar, 3 cm. **e**, An enlarged view of the knitted nanoPE fabric showing the knitted structure. Scale bar, 1.5 mm.

smallest thickness of only 12 μm. The nanoPE fabric with a thickness of 450 μm, about 37 times thicker than the nanoPE thin film, still delivers an infrared transmittance over 70%. Tyvek, a 178-μm-thick non-woven PE textile made by Dupont, shows a little lower mid-infrared transparency than that of the nanoPE fabric. Notably, for a common cotton fabric with a similar thickness to the nanoPE
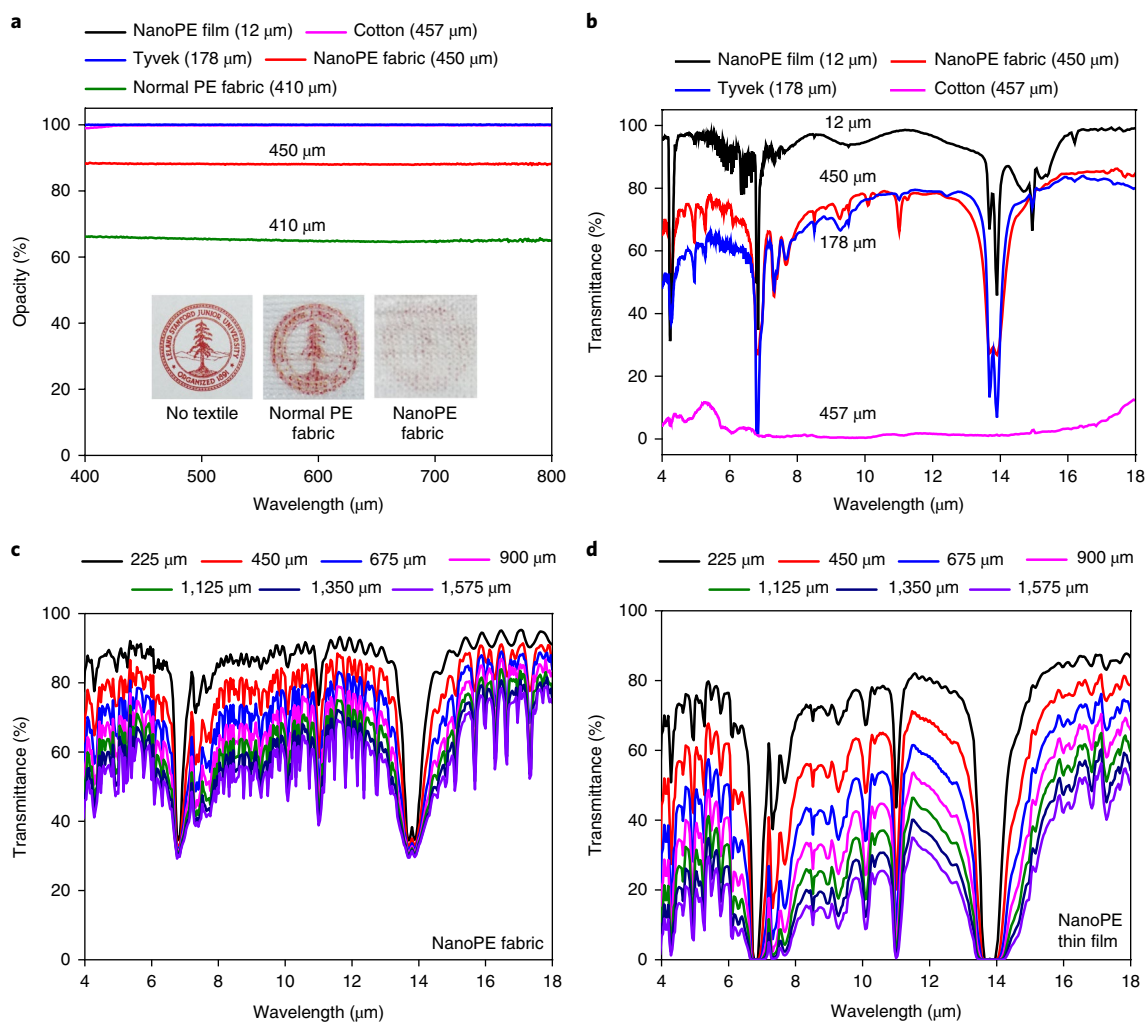
Fig. 3 | Optical properties of the nanoPE fabric and other textiles. a, Visible opacity measurement of nanoPE fabric (thickness: 450 μm), normal PE fabric (thickness: 410 μm), nanoPE thin film, Tyvek and cotton. The inset shows that the nanoPE fabric has a better opacity than the normal PE fabric. **b**, Measured total FTIR transmittance of nanoPE fabric, nanoPE thin film, Tyvek and cotton, with a thickness, respectively, of 450 μm, 12 μm, 178 μm and 457 μm. **c,d**, The dependence of the mid-infrared transmittance on the textile thickness using rigorous coupled-wave analysis for nanoPE fabrics (**c**) and nanoPE thin films (**d**).

fabric, almost no infrared transmittance is observed due to its strong infrared absorption. Furthermore, the nanoPE fabric exhibits better infrared transmittance than the nanoPE thin film of an identical thickness, which can be justified by the infrared transmittance simulation of the nanoPE fabric and nanoPE thin film with varied thickness using rigorous coupled-wave analysis[23]. The dependence of mid-infrared transmittance on the textile thickness is respectively shown in Fig. 3c for the nanoPE fabric and Fig. 3d for the nanoPE thin film. As the thickness increases, the mid-infrared transmittance of the nanoPE fabric and that of the nanoPE thin film both decreases, but the transmittance of the nanoPE fabric decreases less rapidly than that of the nanoPE thin film. With a thickness of 900 μm, the infrared transmittance of the nanoPE thin film drops to less than 30%, while the nanoPE fabric still shows an infrared transmittance of over 60%. This difference clearly demonstrates the advantage in the cooling capacity of the nanoPE fabric over the nanoPE thin film.

To visualize the infrared transmission through various textiles, a thermal camera is employed to detect the infrared radiation transmitting from a simulated human skin. As demonstrated in Fig. 4a, cotton fabric is non-transparent to infrared radiation, and thus the

infrared camera receives the least amount of infrared radiation. Therefore, the thermal imaging of cotton appears the coldest among the samples. The nanoPE thin film and the nanoPE fabric allow most of the infrared radiation to transmit, which can greatly improve the heat loss from the human body. Moreover, the cooling effect of the nanoPE fabric is experimentally demonstrated with an artificial skin temperature measurement (Supplementary Fig. 12). With a similar thickness to the cotton fabric, the nanoPE fabric merely increases the skin temperature by 1.3 °C, while the cotton fabric increases the skin temperature by 3.6 °C (Fig. 4b). The set-point increase of indoor temperature corresponds to the decrease of simulated skin temperature (see Supplementary Note 2 for a more detailed explanation). This difference indicates that people who wear the nanoPE fabric can increase the set-point by 2.3 °C but still feel as thermally comfortable (that is, having the same skin temperature) as the ones who wear cotton clothes. Despite the much larger thickness, the cooling effect of the nanoPE fabric is still comparable to that of the nanoPE thin film. This is potentially due to the desirable convective cooling effect arising from the interlaced structure. Perhaps for the same reason, Tyvek does not show as effective a cooling effect as the nanoPE fabric, even though they display similar mid-infrared transmittances.
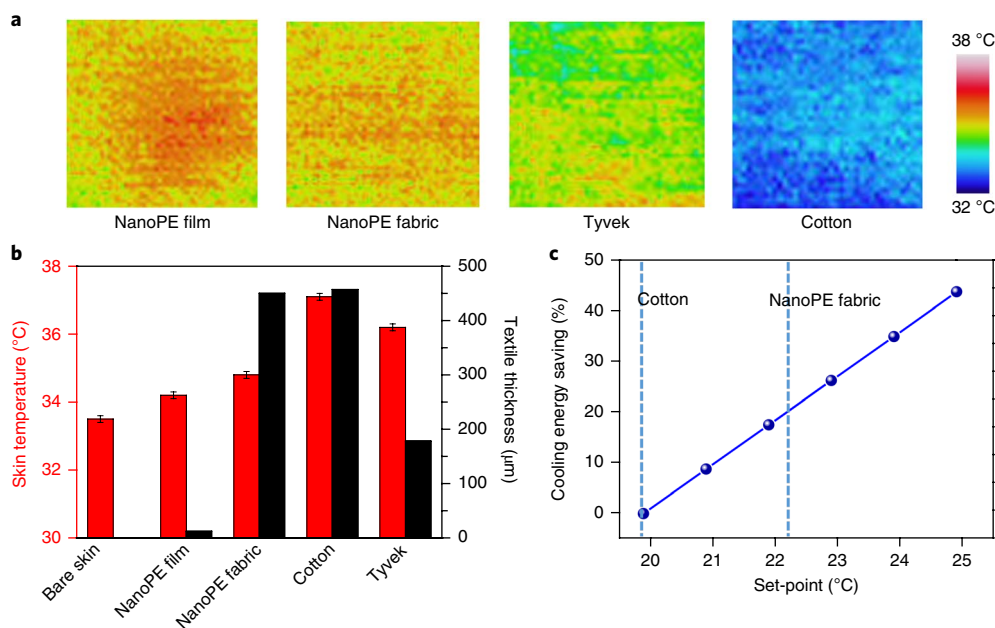
Fig. 4 | Thermal measurement of the nanoPE fabric and other textiles. a, Infrared images of the nanoPE fabric, nanoPE film, Tyvek and cotton on a simulated human skin. **b**, Artificial skin temperature measurement of bare skin, the nanoPE fabric, nanoPE thin film, cotton and Tyvek. The 45-μm-thick nanoPE fabric has a comparable cooling effect to the 12-μm-thick nanoPE thin film. Both are superior to Tyvek and cotton. **c**, Cooling energy saving calculation. As the indoor set-point increases, the cooling energy can be reduced significantly.

The significance of reducing cooling energy consumption via the nanoPE fabric could be quantified (see Supplementary Note 3 for more details). With an increase of indoor set-point, the input cooling energy can be reduced sharply (Fig. 4c). To be more specific, the 2.3 °C set-point difference between the nanoPE fabric and cotton can help save about 20.1% of the cooling energy, which is consistent with results obtained via applying other models[6, 24]. This decrease of energy consumption not only means energy saving, but also suggests CO_2 emission reduction, which is significant in global sustainable development with a wide range of applications.

The nanoPE fabric is primarily designed for an air-conditioned indoor environment for energy saving. The room temperature is usually lower than human body skin temperature in order to realize thermal comfort for the human body. The mid-infrared transparency of the nanoPE fabric provides an additional radiative cooling route to dissipate the majority of heat, besides convection and vaporization, compared with conventional textiles such as cotton. This superior radiative cooling effect can help save a tremendous amount of energy on indoor cooling systems. In addition, the nanoPE fabric may also serve as a potential textile for outdoor cooling. Its superior mid-infrared transparency can help it to harvest coldness from the universe even in a hot environment[7, 8, 25].

Wearability properties

Besides the superior cooling effect, a fabric should also possess suitable wearability properties usually associated with traditional clothes, such as high water vapour transmission rate, air permeability, water wicking rate and mechanical strength. First, people prefer fabrics with a high water vapour transmission rate, which allows the moisture on the skin to evaporate during perspiration to alleviate discomfort. As shown in Fig. 5a, the nanoPE fabric has the highest water vapour transmission rate of 0.023 g cm^{-2} h^{-1}), which is higher than that of cotton and the nanoPE thin film with a water vapour transmission rate of 0.015 g cm^{-2} h^{-1}). This advantage is attributed to the structure design of the nanoPE fabric and the nanoscale cavities inside the nanoPE microfibre. The space among the fibres and the ideal channel network of

nanopores greatly facilitate the water vapour transmission. Air permeability, which is a measure of how well a fabric allows the passage of air, is also essential to the performance of wearable fabrics. Experimentally, the pressure drop as a function of air flow rate of a given fabric area is studied. Cotton, a renowned breathable fabric, transmits air with almost zero pressure drop. The nanoPE fabric presents an equal air permeability to cotton. However, both the nanoPE thin film and Tyvek display poor air permeability (Fig. 5b). Furthermore, the water wicking rate is critical for wearable textile, especially for next-to-skin clothes, which would be wetted by body perspiration. A higher water wicking rate can expedite the sweat transportation and evaporation from human skin. Even though perspiration is not very common in an indoor environment, the water-wicking rate of the nanoPE fabric can be enhanced through facile modification even though PE is intrinsically hydrophobic. We chemically altered its surface property through short-time treatment with a benign hydrophilic and bio-compatible agent, polydopamine. The polar groups –OH and –NH– make the nanoPE fabric hydrophilic[26–28], and additional sparse cotton mesh can further elevate the capillary force for a further improvement of the fabric water-wicking rate. The modified nanoPE fabric demonstrates a wicking rate up to 3 cm per 30 s, approaching that of cotton at around 4 cm per 30 s (Fig. 5c), In addition, adequate mechanical strength of a textile is necessary. Figure 5d shows that the 1.5-cm-wide nanoPE fabric can bear a tensile force of about 15 N, which is satisfactory for human cloth fabrication and almost twice that of the nanoPE thin film[11]. Moreover, the ultimate load of the nanoPE fabric is increased to over 40 N via the addition of a cotton mesh, which is stronger than that of Tyvek and cotton with ultimate loads of approximately 35 N.

The durability and washability of the nanoPE fabric is also tested via a commercial washing and drying machine. After a regular duration of continuous washing and drying (Supplementary Fig. 13a,b), the nanoPE fabric stays intact (Supplementary Video 5 and Supplementary Fig. 13c,d). The nanoPE fabric is durable for multiple cycles of washing and drying, maintaining high
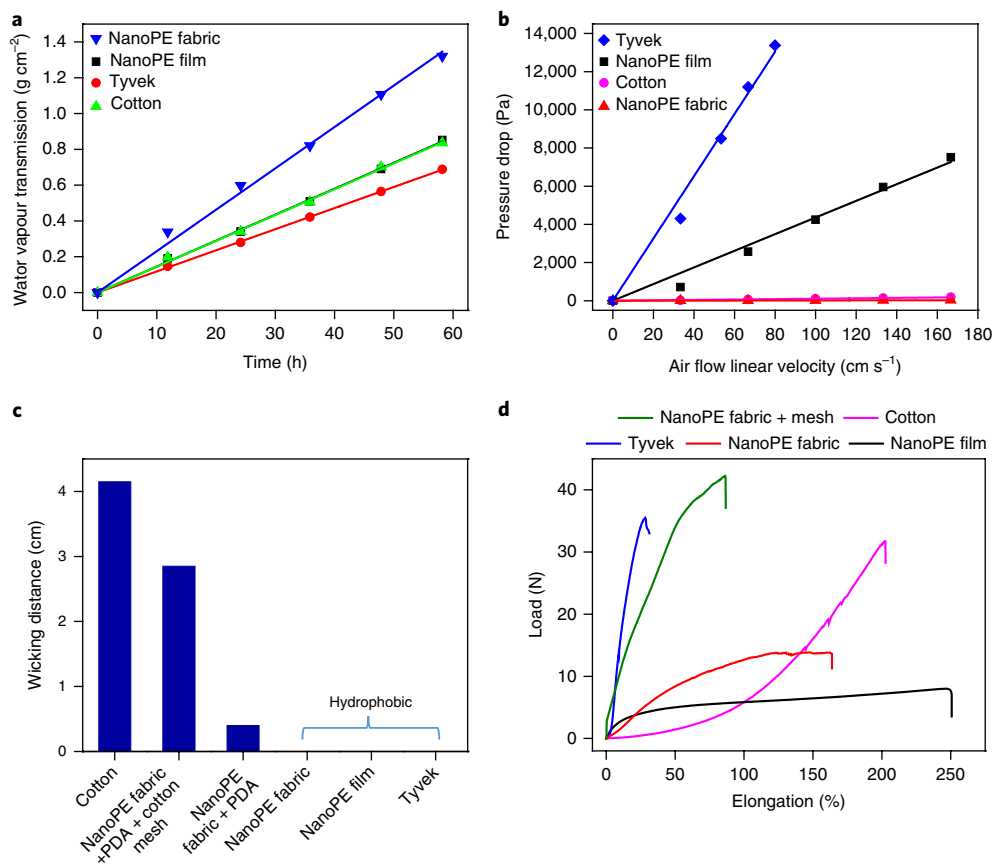
Fig. 5 | Wearability tests for the nanoPE fabric and other textiles. a, A water vapour transmission rate test showing the speed of perspiration transmission through the textile from human skin. **b**, An air permeability test measuring how well the textile allows the passage of air. **c**, A water-wicking test showing the textile capability for perspiration absorbance, transportation and evaporation. **d**, A mechanical strength test showing the relationship between tensile load and elongation.

mid-infrared transmittance (Supplementary Fig. 13e). For the purposes of clothing fashion, the white nanoPE fabric could be coloured by mixing the PE with a very small amount of biocompatible pigment without compromising its mid-infrared transmittance. Further study on the coloration is looking for solutions.

Summary

In summary, we report an energy-saving fabric constructed from nanoPE microfibres using economically viable materials and industrial fabrication technologies. The embedding of nanocavities into the PE microfibre not only ensures the visible opacity, but also achieves cotton-like softness. Compared with the commercial cotton fabric, the nanoPE fabric's superior cooling effect brings about a 2.3 °C drop of the indoor set-point, which corresponds to a 20% energy saving. Besides the enticing cooling effect, the nanoPE fabric also exhibits a collection of compelling wearability features. With large-scale production, it can be immediately and extensively adopted as a sustainable energy-saving solution to improve our way of living. We expect that the nanoPE fabric will not only revolutionize textile for radiative cooling, but also achieve a breakthrough in reducing energy consumption for global sustainability.

Methods

Textile preparation. There were two methods for nanoPE microfibre production. The nanoPE microfibre used in the nanoPE fabric was produced by an extruder (SJ25/25 Plastic Lab Extruder). Before feeding in materials, the extruder was preheated for 1 h until the temperatures of four heating zones were stable at 180 °C

(mould zone 1), 230 °C (barrel zone 3), 230 °C (barrel zone 2) and 230 °C (barrel zone 1). Fibres of various recipes were all produced through the same process. For example, for the nanoPE fabric sample for characterization, we adopted the '1:3.5' recipe (1 g PE with 3.5 ml paraffin oil) to produce fibres. Thirty-five millilitres of paraffin oil (Fisher Scientific), in which 0.078 g antioxidant (Irganox 1010, BASF) was dissolved, and 10 g HDPE (pellets, melt index: 2.2 g per 10 min, Sigma Aldrich) were fed in at the inlet as raw materials. After maintaining a suitable rotation speed for a while, the roller was turned on to collect the fibre when the mixture of HDPE and paraffin oil was extruded out from the outlet of the mould. The fibre was quenched by air. The diameter of the fibre was adjustable by controlling the rotation speed of the main motor and winding machine. All of the fibres were transferred to bobbins, sent to Kimbrell Campus and Textile Technology Center at Gaston College (North Carolina, USA), and knitted/woven there by industrial equipment. The paraffin oil was extracted by methylene chloride (Fisher Scientific) after the fabric was finished. The other way to produce nanoPE microfibres was using multi-filament extrusion at Hills Inc. (North Carolina, USA). The other textile samples are all commercially available: nanoPE thin film (Teklon, 12 μm, Entek International LLC), cotton fabric (single jersey cotton, 130 g m⁻²) and Tyvek (7 mil, Dupont).

Sample characterization. The photograph of the nanoPE fibres and normal PE fibres was taken with an optical microscope (Olympus). The SEM images were taken by an FEI XL30 Sirion SEM (5 kV). The infrared transmittance was measured by an FTIR spectrometer (Model 6700, Thermo Scientific) accompanied with a diffuse gold integrating sphere (PIKE Technologies). The visible opacity was measured by an ultraviolet–visible spectrometer (Agilent, Cary 6000i).

Visible-light scattering simulation. When a beam of light hits an object, it will be scattered in all directions (Supplementary Fig. 11a). The opacity is defined as $(1 - \text{specular transmittance})$[11]. Both diffusive transmission and back reflection help prevent the object from being recognized; thus, both contribute to opacity. Using Mie theory for cylinders[29], the differential scattering cross-section versus

different scattering angles can be obtained (Supplementary Fig. 11b). As an initial estimation, for a human observer with an eye aperture of 1 cm standing at a regular distance of 1 m from another human wearing the fabric, the specular angle can be defined as being within the scattering angle of 0.01 rad, with the rest being diffusive. The calculated differential scattering cross-section as a function of diffraction angle is shown in Supplementary Fig. 11b. Integrating over the angle, the resulting 'specular' and 'diffuse' cross-sections defined above versus wavelength in the visible-light range are shown in Supplementary Fig. 11c, respectively. Finally, the opacity was calculated as: opacity $= 1 - (T_{tot} - T_{dif}) = 1 - ((1 - m\overline{\sigma}_b) - m\overline{\sigma}_{f,dif})$. Here m is the density of the fibres, $\overline{\sigma}_b$ is the total backscattering cross-section and $\overline{\sigma}_{f,dif}$ is the total diffusive forward-scattering cross-section. Inserting numbers as $m = 0.008\,\mu m^{-1}$, $\overline{\sigma}_b = 14.65\,\mu m$, $\overline{\sigma}_{f,dif} = 52.76\,\mu m$, the opacity of the normal PE fabric is 54%.

Simulation of thickness-dependent mid-infrared transmittance. We simulated the infrared transmittance of the nanoPE fabric and the nanoPE film with varied thickness using rigorous coupled-wave analysis. Each fibre is modelled as a round cylinder, and the fabric is formed by a periodic array of fibres. As the infrared wavelength is much larger than the size of the nanopores, we used effective-medium material parameters in simulating nanoPE textiles; that is $\varepsilon_{nanoPE} = (1 - \eta)\varepsilon_{PE} + \eta\varepsilon_{air}$, where η is the porosity.

Thermal measurement. We used a silicone-rubber/fibreglass-insulated flexible heater (Omega, 72 cm²) that was connected to a power supply (Keithley 2400). A ribbon-type hot-junction thermocouple (0.3 mm in diameter, K-type, Omega) was in contact with the top surface of the simulated skin to measure the skin temperature. Another heater the same as the simulated skin was placed below the simulated skin to act as a guard heater. The temperature of the guard heater was always set the same as the skin heater, to ensure the heat flux of simulated skin is only upwards. A thermocouple was in contact with the bottom surface of the guard heater. All of the device was enclosed in a chamber, and the air temperature (ambient temperature) in the chamber was monitored by a third thermal couple and controlled at 23.5 °C by a circulating water heater/chiller. The heating power of the skin heater was set to be 95 W m⁻², which rendered the skin temperature of 33.5 °C when the ambient temperature was 23.5 °C. During measurements, the simulated skin was covered with textile samples (5.5 × 4.5 cm²). The textile sample blocked the heat transfer from the skin heater to the ambient environment, so the skin temperature increased. We set the temperature of the guard heater to be the same as the temperature of the skin heater. The temperature regulation of the guard heater was applied with much caution to ensure the temperature of the guard heater was never higher than that of the skin heater. When their temperatures were the same and stable for 20 min, we read the displayed temperature as the temperature data. The ambient temperature in the measurements was stabilized at 23.5 °C ± 0.1 °C. The thermal images were taken by a calibrated thermal camera (MikroSHOT, Mikron).

Water vapour transmission rate test. The testing procedure was based on ASTM E96 with modification. Medium bottles (100 ml; Fisher Scientific) were filled with 80 ml of distilled water, and sealed with the textile samples using open-top caps and silicone gaskets (Corning). The exposed area of the textile was 3 cm in diameter. The sealed bottles were placed into an environmental chamber in which the temperature was held at 35 °C. The mass of the bottles and the samples was measured periodically. By dividing the reduced mass of the water by the exposed area of the bottle (3 cm in diameter), the water vapour transmission rate was calculated.

Air permeability test. The testing procedure was based on ASTM D737 with modification. The textile sample was fixed between two pipes using double-side tape with a 0.5 cm² exposed area, and the pipe joint was sealed well to ensure its airtightness. One pipe was connected to a T-connector at the short/straight leg and then connected to the compressed air source. A flowmeter (Dwyer, maximum flow rate: 5 l min⁻¹) was placed between the compressed air source and the T-connector. The other pipe was also connected to a T-connector at the short/straight leg and then connected to open air. A differential pressure gauge (UEi Test Instruments) was connected to both long/branch legs to measure the pressure drops across the textile sample at different air flow rates. The linear velocity of the air flow was calculated using the air flow rate divided by the 0.5 cm² exposed area.

Wicking test. The testing procedure was based on AATCC TM 197 with modification. The textile samples were cut into 1-cm-wide strips and dipped into distilled water. Several drops of ink were added to the water for the convenience of observation. We measured the climbing distance of the water in the duration of 30 s. As for the modification of the nanoPE fabric sample, a polydopamine coating solution was prepared firstly. The polydopamine coating solution was made by dissolving dopamine hydrochloride (2 g l⁻¹, Sigma-Aldrich) in Tris buffer solution (10 mM, pH 8.5, Teknova). Then the nanoPE fabric sample was soaked in the coating solution for 1 h to make the surface hydrophilic. A cotton mesh with an opening of 1 × 1 cm² was attached on the above sample to enhance the capillary force.

Mechanical test. The tensile strength test was measured by an Instron 5565. For the mechanical test for the textile samples, the sample size was 1.5 cm wide and 3 cm long, and the gauge distance was 1 cm long. The 'nanoPE fabric + mesh' was prepared by attaching a cotton mesh with an opening of 1 × 1 cm² to the nanoPE fabric sample. For the mechanical test for the fibres of various recipes, one sample contained ten 5-cm-long fibres aligned carefully, and the gauge distance was 3 cm long. The displacement rate was 20 mm min⁻¹.

Bending test. The bending test was conducted by TA instrument Q800 dynamic mechanical analysis in dual-cantilever mode. Normal PE microfibres and nanoPE microfibres are all 170 μm ± 20 μm in diameter. The tested samples were fibre arrays with 30 fibres, and were 7 cm in length and 1.5 cm in width. The frequency sweeping range was 1 Hz–10 Hz.

Porosity measurement. The porosity measurement was based on Archimedes' principle. An object with higher density than water was sunk into distilled water. The increased volume (V_1) was measured, which shall equal the volume of the object. The fibres were weighted and then immerged together with the object into the water. The increased volume (V_2) was again measured, and the volume of the fibres was expressed as $V_2 - V_1$. The bulk density of the nanoPE fibres (ρ_{nano}) can therefore be calculated. Note, the PE fibres are hydrophobic, so the water cannot enter the nanopores. The density of normal, non-porous PE fibres (ρ_{normal}) was also measured with the same method. The porosity (ϕ) of nanoPE fibres is calculated as $\phi = 1 - \rho_{nano}/\rho_{normal}$.

Data availability. The data that support the findings of this study are available from the corresponding author upon request.

References

1. King, D. A. Climate change science: adapt, mitigate, or ignore? *Science* **303**, 176–177 (2004).
2. Chu, S. & Majumdar, A. Opportunities and challenges for a sustainable energy future. *Nature* **488**, 294–303 (2012).
3. Roemmich, D. et al. Unabated planetary warming and its ocean structure since 2006. *Nat. Clim. Change* **5**, 240–245 (2015).
4. Lee, R. The outlook for population growth. *Science* **333**, 569–573 (2011).
5. Goldstein, E. A., Raman, A. P. & Fan, S. Sub-ambient non-evaporative fluid cooling with the sky. *Nat. Energy* **2**, 17143 (2017).
6. Hoyt, T., Arens, E. & Zhang, H. Extending air temperature setpoints: simulated energy savings and design considerations for new and retrofit buildings. *Build. Environ.* **88**, 89–96 (2015).
7. Raman, A. P., Anoma, M. A., Zhu, L., Rephaeli, E. & Fan, S. Passive radiative cooling below ambient air temperature under direct sunlight. *Nature* **515**, 540–544 (2014).
8. Kou, J., Jurado, Z., Chen, Z., Fan, S. & Minnich, A. J. Daytime radiative cooling using near-black infrared emitters. *ACS Photonics* **4**, 626–630 (2017).
9. Zhai, Y. et al. Scalable-manufactured randomized glass-polymer hybrid metamaterial for daytime radiative cooling. *Science* **355**, 1062–1066 (2017).
10. Hsu, P.-C. et al. Personal thermal management by metallic nanowire-coated textile. *Nano. Lett.* **15**, 365–371 (2014).
11. Hsu, P.-C. et al. Radiative human body cooling by nanoporous polyethylene textile. *Science* **353**, 1019–1023 (2016).
12. Tong, J. K. et al. Infrared-transparent visible-opaque fabrics for wearable personal thermal management. *ACS Photonics* **2**, 769–778 (2015).
13. Hardy, J. D. & Dubois, E. F. Regulation of heat loss from the human body. *Proc. Natl Acad. Sci. USA* **23**, 624–631 (1937).
14. Chen, J. & Wang, Z. L. Reviving vibration energy harvesting and self-powered sensing by a triboelectric nanogenerator. *Joule* **1**, 480–521 (2017).
15. Viklund, C., Svec, F. & Frechet, J. M. J. Monolithic, "molded", porous materials with high flow characteristics for separations, catalysis, or solid-phase chemistry: control of porous properties during polymerization. *Chem. Mater.* **8**, 744–750 (1996).
16. Rogers, J. A., Someya, T. & Huang, Y. Materials and mechanics for stretchable electronics. *Science* **327**, 1603–1607 (2010).
17. Khang, D.-Y., Jiang, H., Huang, Y. & Rogers, J. A. A stretchable form of single-crystal silicon for high-performance electronics on rubber substrates. *Science* **311**, 208–212 (2006).
18. Ahn, B. Y. et al. Omnidirectional printing of flexible, stretchable, and spanning silver microelectrodes. *Science* **323**, 1590–1593 (2009).
19. Fang, X., Wyatt, T., Hong, Y. & Yao, D. Gel spinning of UHMWPE fibres with polybutene as a new spin solvent. *Polym. Eng. Sci.* **56**, 697–706 (2016).
20. Ruan, S., Gao, P. & Yu, T.-X. Ultra-strong gel-spun UHMWPE fibers reinforced using multiwalled carbon nanotubes. *Polymer* **47**, 1604–1611 (2006).
21. Samon, J. M., Schultz, J. M. & Hsiao, B. S. Structure development in the early stages of crystallization during melt spinning. *Polymer* **43**, 1873–1875 (2002).
22. Ihm, D., Noh, J. & Kim, J. Effect of polymer blending and drawing conditions on properties of polyethylene separator prepared for Li-ion secondary battery. *J. Power Sources* **109**, 388–393 (2002).

23. Liu, V. & Fan, S. S4: A free electromagnetic solver for layered periodic structures. *Comput. Phys. Commun.* **183**, 2233–2244 (2012).
24. Ghahramani, A., Zhang, K., Dutta, K., Yang, Z. & Gerber, B. Energy savings from temperature setpoints and deadband: Quantifying the influence of building and system properties on savings. *Appl. Energy* **165**, 930 (2016).
25. Chen, Z., Zhu, L., Raman, A. & Fan, S. Radiative cooling to deep sub-freezing temperatures through a 24-h day–night cycle. *Nat. Commun.* **7**, 13729 (2016).
26. Lee, H., Dellatore, S. M., Miller, W. M. & Messersmith, P. B. Mussel-inspired surface chemistry for multifunctional coatings. *Science* **318**, 426–430 (2007).
27. Ryu, J., Ku, S.-H., Lee, H. & Park, C. B. Mussel-inspired polydopamine coating as a universal route to hydroxyapatite crystallization. *Adv. Funct. Mater.* **20**, 2132–2139 (2010).
28. Ryou, M.-H., Lee, Y. M., Park, J.-K. & Choi, J.W. Mussel-inspired polydopamine-treated polyethylene separators for high-power Li-ion batteries. *Adv. Mater.* **23**, 3066–3070 (2011).
29. Kerker, M. & Matijević, E. Scattering of electromagnetic waves from concentric infinite cylinders. *J. Opt. Soc. Am.* **51**, 506–508 (1961).

Acknowledgements

Author contributions

Y.P., J.C. and Y.C. conceived the idea, planned the study, designed the experiment, analysed the data and composed the manuscript. Y.P. and J.C. performed all of the experiments with the assistance of P.-C.H., L.C., B.L., G.Z., D.S.W. and H.R.L. Y.P. and J.C. addressed all of the reviewers' concerns together. A.Y.S. performed the optical simulation. Y.Z. performed the energy saving calculation. P.B.C. coordinated the project. Y.C. and S.F. supervised the project. All of the authors reviewed and commented on the manuscript.

Competing interests

Y.C., S.F., Y.P., J.C., A.Y.S., P.B.C. and P.-C.H. have a US patent application No. 62/399,974 related to this work.

Additional information

Supplementary information accompanies this paper at https://doi.org/10.1038/s41893-018-0023-2.

Reprints and permissions information is available at www.nature.com/reprints.

Correspondence and requests for materials should be addressed to Y.C.

Publisher's note: Springer Nature remains neutral with regard to jurisdictional claims in published maps and institutional affiliations.